Modeling and design of a multivariable control system for multi-paralleled grid-connected inverters with LCL filter

Akhavan, Ali; Mohammadi, Hamid Reza; Guerrero, Josep M.

Published in:
International Journal of Electrical Power and Energy Systems

DOI (link to publication from Publisher):
10.1016/j.ijepes.2017.07.016

Publication date:
2018

Document Version
Early version, also known as pre-print

Modeling and Design of a Multivariable Control System for Multi-Paralleled Grid-Connected Inverters with *LCL* Filter

Ali Akhavan, Hamid Reza Mohammadi, and Josep M. Guerrero

Abstract—The quality of injected current in multi-paralleled grid-connected inverters is a matter of concern. The current controlled grid-connected inverters with *LCL* filter are widely used in the distributed generation (DG) systems due to their fast dynamic response and better power features. However, designing a reliable control system for grid-connected inverters with *LCL* filter is complicated. Firstly, overcoming to system resonances due to *LCL* filters is a challenging task, intrinsically. This could become worse as number of paralleled grid-connected inverters increased. In order to deal with resonances in the system, damping methods such as passive or active damping is necessary. Secondly and perhaps more importantly, paralleled grid-connected inverters in a microgrid are coupled due to grid impedance. Generally, the coupling effect is not taken into account when designing the control systems. In consequence, depending on the grid impedance and the number of paralleled inverters, the inverters installed in a microgrid do not behave as expected. In other words, with a proper control system, a single inverter is stable in grid-connected system, but goes toward instability with parallel connection of other inverters. Therefore, consideration of coupling effect in the multi-paralleled grid-connected inverters is vital. Designing control systems for multi-paralleled grid-connected inverters becomes much more difficult when the inverters have different characteristics such as *LCL* filters and rated powers. In this paper, the inverters with different characteristics in a microgrid are modeled as a multivariable system. The comprehensive analysis is carried out and the coupling effect is described. Also, the control system design for multi-paralleled grid-connected inverters with *LCL* filter is clarified and a dual-loop active damping control with capacitor current feedback is designed. Finally, the proposed multivariable control system for a microgrid with three-paralleled grid-connected inverters with *LCL* filter is validated by simulation.

Keywords: Multi-paralleled inverters, Active damping, Coupling effect, *LCL* filter

1. Introduction

Renewable energy is harvested from nature, it is clean and free. However, it is widely accepted that renewable energy is not a panacea that comes without challenges. As an interface between the distributed generation (DG) plants and the grid, the grid-connected inverters are essential to convert all kinds of generated power into a high quality AC power and inject it into the grid reliably [1]. The inverters installed in microgrids are generally voltage source inverters with an output filter. Nowadays, the *LCL* filter is considered to be a preferred choice for attenuation of switching frequency harmonics in the injected grid current compared with the *L* filter [2], [3]. Because of using smaller reactive elements, the cost and weight of the inverter system are reduced when using *LCL* filter. However, due to the resonance of the *LCL* filter, damping methods are needed for the grid-connected inverters to stabilize the system [4]. Passive and active methods for damping the resonance of the *LCL* filter have been extensively discussed in literature [5]–[8]. Active damping is preferred to passive damping due to its high efficiency and flexibility of the conversion.

The quality of the grid injected current is very important in the grid-connected systems. International standards regulate the connection of inverters to the grid and limit the harmonic content of the injected current. IEEE std. 1547-2003 [9] gives the limitation of the injected grid current harmonics. If the harmonic content of the injected current exceeds the standard limits, it is required to disconnect the inverter from the grid. Thus, the *LCL* filters are implemented to prevent the grid from being polluted with switching harmonics. Therefore, designing adequate control system for grid-connected inverters with *LCL* filter is a matter of concern.

A more difficulty is appeared when multi-paralleled grid-connected inverters are coupled due to the grid impedance Z_g. In this condition, the inverters influence each other as a result. All inverters in Fig. 1, share the voltage in the point of common coupling (PCC) V_{pcc} and are able to modify this voltage by injecting their currents [10]. It should be noted that, if the grid impedance was ideally considered to be zero, the coupling effect would not exist because the voltage in the PCC would always be V_g. Depending on the number of paralleled inverters and the grid impedance Z_g, the inverters installed in a microgrid might not behave as

expected. In other words, with proper control system, a single inverter is stable in grid-connected system, but goes toward instability with parallel connection of other inverters. Therefore, consideration of coupling effect in the multi-paralleled grid-connected inverters is very important and microgrid should be modeled as a multivariable system.

Many literatures with regard to active damping strategies are published [11]-[18]. However, their analyses are done for single grid-connected inverter. In consequence, coupling effect among inverters due to grid impedance is not considered and the stability and performance of the inverter in a microgrid might be questioned. In [10], authors have been modeled the *N*-paralleled inverters in a PV power plant as a multivariable system. However, all inverters are assumed to be the same including their hardware, software, rated powers, *LCL* filters and reference injected currents. It is widely accepted that this assumption is not valid in the real microgrid since different sources such as photovoltaic panels, wind turbines and fuel cells with different inverters, *LCL* filters and reference injected currents may be collected in a microgrid. Also, in case of PV power plants as considered in [10], even though the same panels and inverters are used, the reference current of each inverter may be different due to partial shadow. In [19], a robust control strategy for a grid-connected multi-bus microgrid containing several inverter-based DG units is proposed. However, only compensation of positive and negative sequence current components using Lyapunov function and sliding mode method is discussed. In [20], a back to back (B2B) converter connection is proposed to provide a reliable interface, while it can provide isolation between utility and microgrids.

In this paper, modeling and control of three-paralleled grid-connected inverters with different characteristics are described. In fact, the *LCL* filter parameters, rated powers and also, reference injected currents of the inverters are considered to be different. For this task, all inverters are modeled as a multivariable system in order to modeling the coupling effect among inverters due to grid impedance. Also, dual-loop active damping control using the capacitor current feedback as inner loop [5] is chosen for its simple and effective implementation. Due to single phase application, the proportional and resonant (PR) controllers are considered for control system.

This paper is organized as follows. In Section 2, modeling and control of a single grid-connected inverter is described. In Section 3, modeling and control of the three-paralleled grid-connected inverters with different characteristics in a microgrid are analyzed. In Section 4, controller design regarding to PR controllers for the multivariable system that is modeled in previous section is described. In Section 5, the theoretical study is validated through simulation in MATLAB software. Finally, Section 6, concludes this paper.

2. Modeling and Control of a Single Grid-Connected Inverter

In this section, the modeling and control of a single grid-connected inverter with *LCL* filter is described. Although, this issue has already been addressed in available literatures [11]-[17], the goal is to get the reader familiarized with the methodology used along this paper.

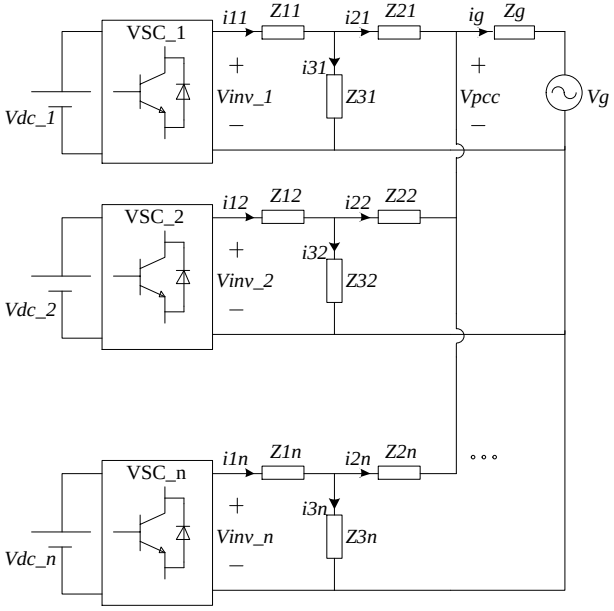

Fig. 1. Typical multi-paralleled grid-connected inverters.

A generic structure of the *LCL*-filtered grid-connected inverter is shown in Fig. 2. The *LCL* filter consists of an inverter-side inductor L_1, a filter capacitor C, and a grid-side inductor L_2. Parasitic resistances are neglected in order to simplicity.

$$Z_1 = L_1.s,\ Z_2 = L_2.s,\ Z_3 = \frac{1}{C_3.s},\ Z_g = L_g.s \tag{1}$$

In this figure, V_{dc} is the input DC voltage, V_{inv} is the output voltage of the inverter bridge, i_1, i_g, i_C are inverter-side current, grid-side current and capacitor current, respectively. Also, $G_i(s)$ is the current regulator and i_C is fed back to damp the *LCL* filter resonance. At the PCC, the grid is modeled by its Thevenin equivalent circuit for simplicity, consisting of a voltage source V_g in series with grid impedance Z_g. $G_d(s)$ is the transfer function which combines the computational delay, the PWM delay, and the sampler [10].

$$G_d(s) = \frac{1 - 0.5.s.T_s}{(1 + 0.5.s.T_s)^2} \tag{2}$$

Where, T_s refers to the sampling period.

With the aforementioned model, the linearized model of the single grid-connected inverter with *LCL* filter in *s*-domain can be derived as shown in Fig. 3(a). In this figure, K_{PWM} is the proportional controller in the inner loop. Considering Fig. 3(a), adequate controller design is quite complicate due to interacting loops and complexity of the system. To simplify the design procedure, an equivalent model containing decoupled regulating loops would be desirable. The model in Fig. 3(a) can be simplified by adding capacitor voltage (v_C) to output signal of the transfer function K_{PWM}, and by replacing feedback signal i_C with i_1-i_g. In this way, the equivalent model of the system will be obtained as shown in Fig. 3(b). Now, the design procedure can be done considering decoupled loops. It is well known that the cut-off frequency of the inner loop must be higher than the outer loop.

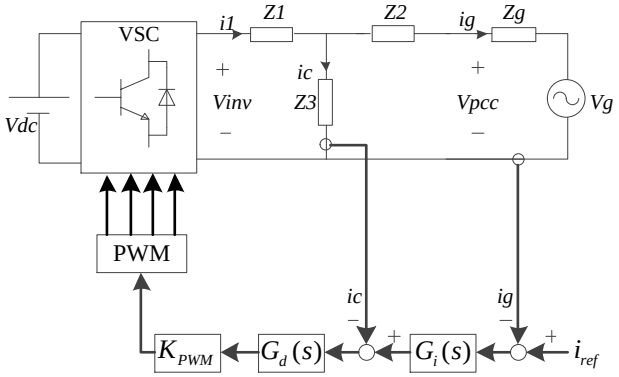

Fig. 2. Configuration of a single grid-connected inverter with *LCL* filter.

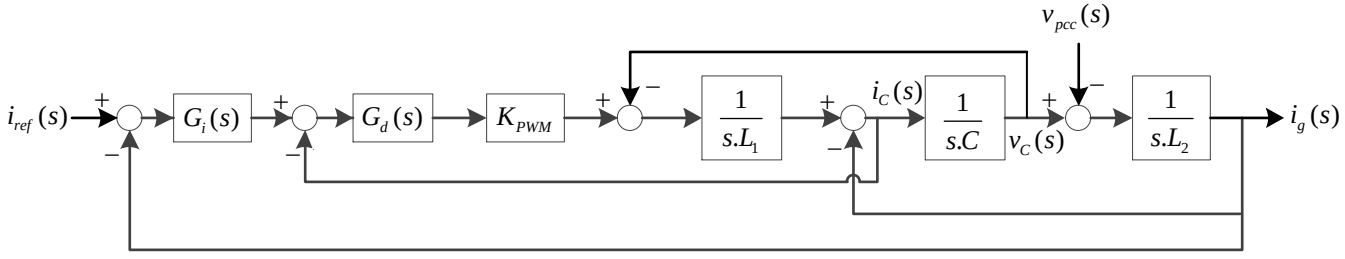

(a)

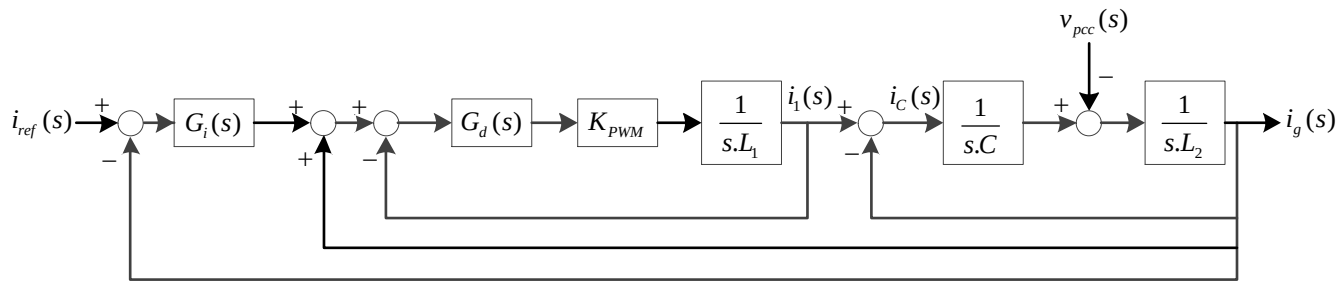

(b)

Fig. 3. (a) Block diagram of the dual-loop control strategy based on capacitor current feedback. (b) Simplified block diagram of the aforementioned dual-loop control strategy.

3. Modeling and Control of Multi-Paralleled Grid-Connected Inverters

3.1. System Description

A set of *N*-paralleled *LCL*-filtered grid-connected inverters is shown in Fig. 1. The dynamics of these inverters are coupled due to the grid impedance. The equivalent circuit for current control design of the *N*-paralleled inverters of Fig. 1 is shown in Fig. 4, where Z_{1i} (with $i = 1 \ldots N$), Z_{2i} and Z_{3i} are the inverter-side inductor impedances, the grid-side inductor impedances and the capacitor impedances, respectively. Moreover, i_{1i}, i_{2i} and i_{3i} are the inverter side current, the grid side current and the capacitor current, respectively. v_{Z3i} is the capacitor voltage and v_{inv_i} is the inverter output voltage, all for *i-th* inverter. Also, i_g is the grid injected current.

3.2. Modeling

Multivariable control loops corresponding to the three-paralleled grid-connected inverters with *LCL* filter coupled due to the grid impedance in a microgrid are shown in Fig. 5. This is the Multiple Input Multiple Output (MIMO) version of the Single Input Single Output (SISO) control loop of Fig. 3(b). In this figure, $\bar{G}_i(s)$ is the matrix transfer function that contains the controllers $G_i(s)$; $\bar{G}_d(s)$ is the diagonal matrix transfer function that contains the delay transfer function $G_d(s)$; $\bar{K}_{PWM}$ is the matrix transfer function of the inner loop regulators; $\bar{G}(s)$ is the matrix transfer function representing the relation between the inverter-side currents i_{1i} and inverter output voltages v_{inv_i}. Due to coupling effect, this matrix transfer function contains diagonal and non-diagonal elements which will be obtained in the next step.

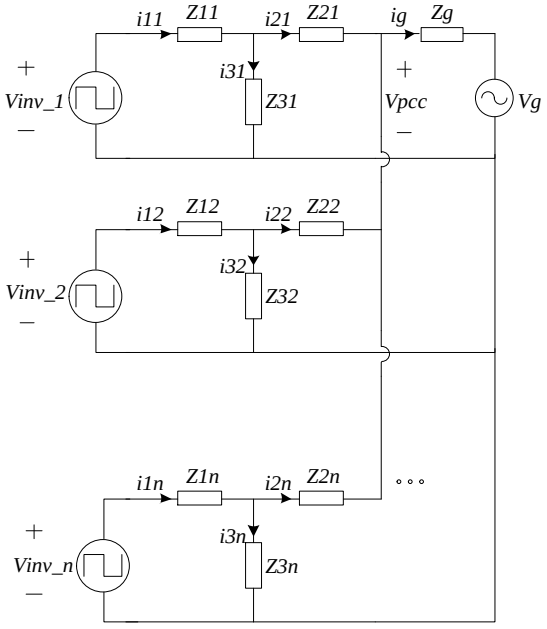

Fig. 4. The equivalent circuit of the *N*-paralleled inverters.

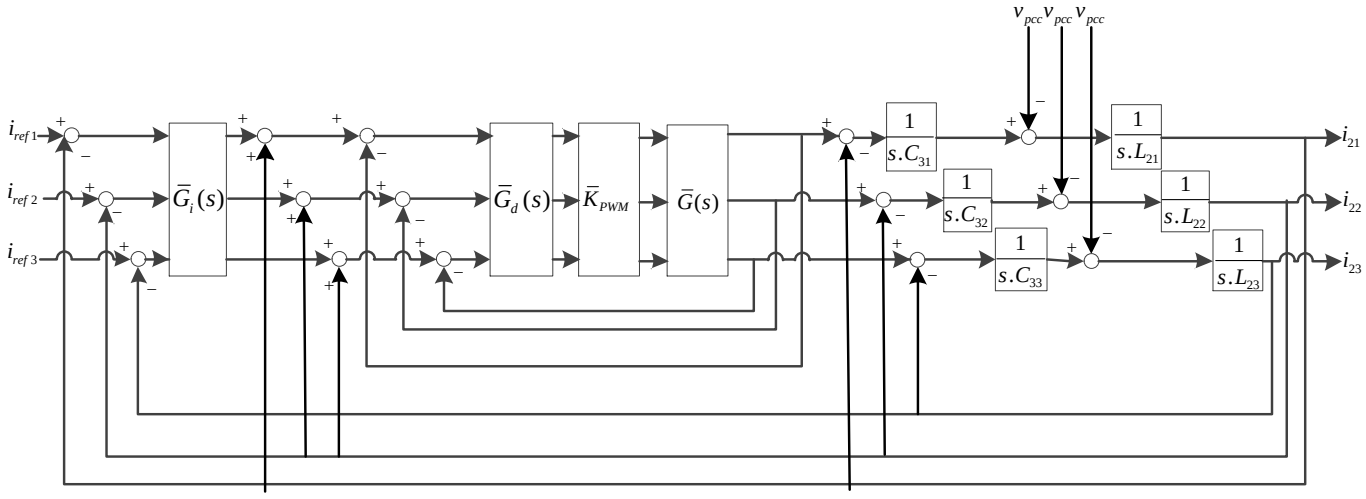

Fig. 5. Multivariable control loops for three-paralleled grid-connected inverters.

3.3. Calculation of the Matrix Transfer Function $\bar{G}(s)$

Matrix transfer function $\bar{G}(s)$ is represented in (3). This matrix has non-diagonal elements since each inverter output voltage v_{inv_i} influences the output current of other inverters. The elements of the matrix transfer function $\bar{G}(s)$ are calculated through the superposition and Thevenin equivalent circuit theorems.

$$\bar{i}_{1n} = \bar{G}(s) \times \bar{v}_{inv}$$
$$\begin{bmatrix} i_{11} \\ i_{12} \\ \dots \\ i_{1n} \end{bmatrix} = \begin{bmatrix} G_{11} & G_{12} & \dots & G_{1n} \\ G_{21} & G_{22} & \dots & G_{2n} \\ \dots & \dots & \dots & \dots \\ G_{n1} & G_{n2} & \dots & G_{nn} \end{bmatrix} \times \begin{bmatrix} v_{inv1} \\ v_{inv2} \\ \dots \\ v_{inv\_n} \end{bmatrix} \quad (3)$$

The diagonal elements are regarded as the transfer functions between the inverter-side current and its own output voltage.

Accordingly, G_{11}, for example, can be calculated if grid voltage and all the inverter output voltages v_{inv_i} are supposed to be zero except v_{inv_1}. For this purpose, the auxiliary circuit of Fig. 6 is derived from Fig. 4. In this circuit, the output current is i_{11} and the only voltage source is v_{inv_1}. Therefore the diagonal element G_{11}, can be directly obtained. Similarly, other elements of the matrix transfer function $\bar{G}(s)$ can be calculated as presented in the Appendix.

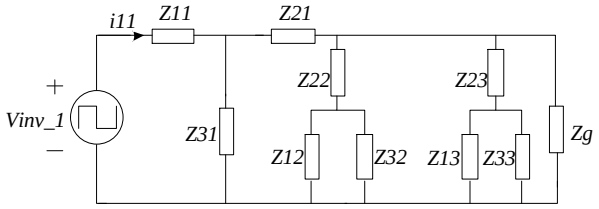

Fig. 6. Auxiliary circuit of the three-paralleled inverters provided that grid voltage and all the converter voltages v_{inv_i} are zero except v_{inv_1}.

4. Control System Design

4.1. Design of Controller for Multivariable System

In order to determine the interaction between loops of a MIMO system, relative gain array (RGA) method can be used [21]. The RGA of a non-singular square matrix $\bar{G}(s)$ is defined as

$$\Lambda = \bar{G}(0).\times \bar{G}(0)^{-T} \quad (4)$$

Where $.\times$ denotes element-by-element multiplication and $\bar{G}(0)$ is the matrix $\bar{G}(s)$ in the steady-state condition (ω=0).

The RGA is a square matrix which has some unique properties, i.e. the sum of its rows as its columns are equal to 1. If diagonal elements of the RGA matrix be close to unity, the system is diagonally dominant. In other words, interaction of loops in the system is relatively low and each output can be controlled by one input. On other hand, in MIMO systems with severe interaction, each output is related to the all inputs. In fact, RGA is an index which shows degree of interaction in a MIMO system. Since in the described control loop only matrix transfer function $\bar{G}(s)$ has non-diagonal elements, therefore, the RGA of this matrix should be calculated.

By using the parameters listed in Table I, the matrix transfer function $\bar{G}(0)$ which contains the transfer functions in the Appendix, is calculated as:

$$\bar{G}(0) = \begin{bmatrix} 1.7757 & -0.3738 & -0.2804 \\ -0.3738 & 2.7103 & -0.4673 \\ -0.2804 & -0.4673 & 2.1495 \end{bmatrix} \quad (5)$$

Therefore, the RGA matrix can be easily calculated as follows:

$$\Lambda = \bar{G}(0).\times \bar{G}(0)^{-T} = \begin{bmatrix} 1.0654 & -0.0374 & -0.0280 \\ -0.0374 & 1.0841 & -0.0467 \\ -0.0280 & -0.0467 & 1.0748 \end{bmatrix} \quad (6)$$

TABLE I
PARAMETERS OF THE INVERTERS AND GRID

Parameters of the inverter1	
Input DC voltage, V_{dc_1}	360 V
Inverter-side impedance Z_{11} (R_{11}, L_{11})	L_{11}=330 µH R_{11}=0.2 Ω
Grid-side impedance Z_{21} (R_{21}, L_{21})	L_{21}=330 µH R_{21}=0.3 Ω
Impedance of filter capacitor Z_{31} (R_{31}, L_{31})	C_{31}=10 µF R_{31}=0.2 Ω
Sampling frequency	30 kHz
Switching frequency	10 kHz
Rated power	5 kVA
Parameters of the inverter2	
Input DC voltage, V_{dc_2}	360 V
Inverter-side impedance Z_{12} (R_{12}, L_{12})	L_{12}=1 mH R_{12}=0.1 Ω
Grid-side impedance Z_{22} (R_{22}, L_{22})	L_{22}=1 mH R_{22}=0.2 Ω
Impedance of filter capacitor Z_{32} (R_{32}, L_{32})	C_{32}=13 µF R_{32}=0.3 Ω
Sampling frequency	30 kHz
Switching frequency	10 kHz
Rated power	5 kVA
Parameters of the inverter3	
Input DC voltage, V_{dc_3}	360 V
Inverter-side impedance Z_{13} (R_{13}, L_{13})	L_{13}=600 µH R_{13}=0.3 Ω
Grid-side impedance Z_{23} (R_{23}, L_{23})	L_{23}=200 µH R_{23}=0.1 Ω
Impedance of filter capacitor Z_{33} (R_{33}, L_{33})	C_{33}=10 µF R_{33}=0.2 Ω
Sampling frequency	30 kHz
Switching frequency	10 kHz
Rated power	10 kVA
Parameters of the grid	
Grid Voltage, V_g (RMS)	220 V
Fundamental frequency f_0	50 Hz
Grid impedance Z_g (R_g, L_g)	L_g=1.3 mH R_g=0.1 Ω

According to the calculated RGA matrix, diagonal elements are close to unity and non-diagonal elements are close to zero. Hence, if cut-off frequency of each main loop designed as high as possible, the interaction of loops can be neglected. It should be noted that with this assumption, the coupling due to the grid impedance remains because any diagonal elements of matrix $\bar{G}(s)$, for example G_{11}, includes the elements of other inverters such as Z_{12}, Z_{22}, Z_{13}, Z_{23} and etc. (See Appendix). However, if in another case study, the diagonal elements of the RGA matrix be far from unity and there is severe interaction in the system, the pre-compensator matrix can be used to reduce the interaction [21].

Corresponding control system for designing the inner loop and outer loop controllers for Inverter1 is shown in Fig. 7. In this figures, G_{11} is the first diagonal elements of $\bar{G}(s)$. It should be noted that, block diagrams of control system for Inverter2 and Inverter3 are not shown due to similarity. For example, to achieving the block diagram of control system for Inverter2, G_{11} should

be replaced by G_{22} (second diagonal elements of $\bar{G}(s)$) and K_{PWM1} should be replaced by K_{PWM2}. Also, blocks that are related to capacitor (C_{31}) and grid-side inductor (L_{21}) of Inverter1, should be replaced by capacitor and grid-side inductor of Inverter2 (i.e. C_{32} and L_{22}, respectively).

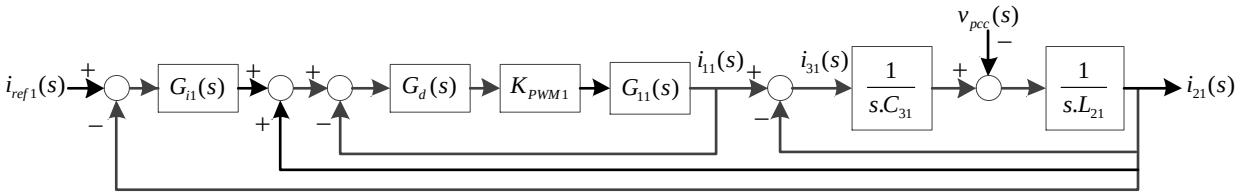

Fig. 7. Block diagram of the control systems of Inverter1.

4.2. PR Controllers

For a three phase converter, a simple PI controller which is designed in the *dq* rotating reference frame, achieves infinite loop gain and consequently zero steady state error at the fundamental frequency. However, this method is not applicable to single-phase converters, because there is only one phase variable available. The *dq* transformation requires a minimum of two orthogonal variables [22], [23]. Hence, in single phase applications, it is common to use PR controller as (7) due to its high gain at the fundamental frequency.

$$G_{PR}(s) = k_p + \frac{k_r s}{s^2 + \omega_0^2} \tag{7}$$

Where, $\omega_0 = 2 \times \pi \times f_0$ and f_0 is the fundamental frequency.

PR controller and also inner loop proportional controller for each control system should be designed using bode diagram and considering phase margin and cut-off frequency constraints. At first, inner loop proportional controller should be designed and then outer loop PR controller can be designed. It is well known that the cut-off frequency of the inner loop must be higher than outer loop.

4.3. Design the Parameters of the Controllers

In this paper, a proportional controller is used as inner loop controller to enhance the cut-off frequency of the inner loop. The loop gain of the inner loop for inverter1 control system, which shown in Fig. 7, can be easily obtained as

$$G_{inner}(s) = G_d(s) \cdot K_{PWM1} \cdot G_{11}(s) \tag{8}$$

If inner loop cut-off frequency defined as ω_{inner}, then proportional controller can be achieved as:

$$\left|G_{inner}\right|_{s=j\omega_{inner}} = \left|G_d(s) \cdot K_{PWM1} \cdot G_{11}(s)\right|_{s=j\omega_{inner}} = 1 \Rightarrow K_{PWM1} = \frac{1}{\left|G_d(s) \cdot G_{11}(s)\right|_{s=j\omega_{inner}}} \tag{9}$$

Afterward, in order to obtain the parameters of PR controller, the control system loop gain should be achieved as follows:

$$G_{ol,sys}(s) = G_{i1}(s) \cdot G_{sys}(s) \tag{10}$$

Where, G_{sys} is the control system loop gain when G_{i1}=1.

$$G_{sys}(s)=\frac{G_d(s)\cdot K_{PWM1}\cdot G_{11}(s)}{1+s^2L_{21}C_{31}+G_d(s)\cdot K_{PWM1}\cdot G_{11}(s)\cdot s^2L_{21}C_{31}} \tag{11}$$

With defining outer loop cut-off frequency as ω_{outer} and regarding to this fact that if $\omega_{outer} > \omega_0$ [24], the PR controller can be simplified as

$$G_{i1}(s)\Big|_{j\omega_{outer}} = G_{PR}(s)\Big|_{j\omega_{outer}} \approx k_p \tag{12}$$

Therefore, k_p can be yield as

$$\left|G_{i1}(s)\cdot G_{sys}(s)\right|_{s=j\omega_{outer}} = 1 \Rightarrow k_p = \frac{1}{\left|G_{sys}(s)\right|_{s=j\omega_{outer}}} \tag{13}$$

Then, with defining a specific phase margin (PM) such as PM_{def}, next equation at cut-off frequency yields.

$$\measuredangle G_{ol,sys}(s)\Big|_{s=j\omega_{outer}} = -180 + PM_{def} \Rightarrow \measuredangle G_{i1}(s)\Big|_{s=j\omega_{outer}} + \measuredangle G_{sys}(s)\Big|_{s=j\omega_{outer}} = -180 + PM_{def} \tag{14}$$

With a bit mathematical simplification, k_r can be achieved as

$$k_r = k_p \cdot \frac{\omega_{outer}^2 - \omega_0^2}{\omega_{outer}} \cdot \tan(\measuredangle G_{sys}(s)\Big|_{s=j\omega_{outer}} + 180 - PM_{def}) \tag{15}$$

Obviously, ω_{inner} should be greater than ω_{outer} in order to decouple inner loop from outer loop.

5. Simulation Results

In this section, a single phase microgrid with three-paralleled grid-connected inverters with *LCL* filter is simulated using MATLAB/SIMULINK software. The simulation results are analyzed so as to validate the theoretical study of previous sections. The key parameters of the inverters are shown in Table I. To show necessity of considering coupling effect in multi-paralleled grid-connected inverters, two different simulations are performed. At first, Set I control parameters listed in Table II is used for simulation. These parameters are designed using bode diagram and without considering the coupling effect of three inverters.

In other words, block diagram which shown in Fig. 3(b) is used for design of controllers of each inverter, individually. The magnitudes of reference injected currents (i_{ref}) of these inverters are 20, 30 and 40A, respectively and the corresponding phase angles are 0°. In Figs. 8(a)-(c), simulation results for single grid-connected inverter are shown for each inverter. As shown in these figures, all three inverters are stable when they are connected to the grid, individually. Total harmonic distortion (THD) of each inverter injected current are 3.50%, 1.22% and 1.05%, respectively. The simulation results for parallel connection of all three inverters to the grid, with previous control parameters, are shown in Figs. 9(a)-(c). As shown in these figures, although the individual connection of each inverter to the grid is stable, parallel connection of inverters to the grid will be unstable. This simulation results show that considering of coupling effect in multi-paralleled grid-connected inverters is necessary.

TABLE II
PARAMETERS OF THE CONTROLLERS

SET I					
Parameters of the controllers of inverter 1		Parameters of the controllers of inverter 2		Parameters of the controllers of inverter 3	
K_{pwm1}	7.35	K_{pwm1}	37.2	K_{pwm1}	15.2
K_p	0.72	K_p	1.29	K_p	0.65
K_r	350	K_r	233	K_r	281
SET II					
Parameters of the controllers of inverter 1		Parameters of the controllers of inverter 2		Parameters of the controllers of inverter 3	
K_{pwm1}	5.37	K_{pwm1}	10.6	K_{pwm1}	6.24
K_p	0.66	K_p	0.34	K_p	0.60
K_r	318	K_r	66.7	K_r	267

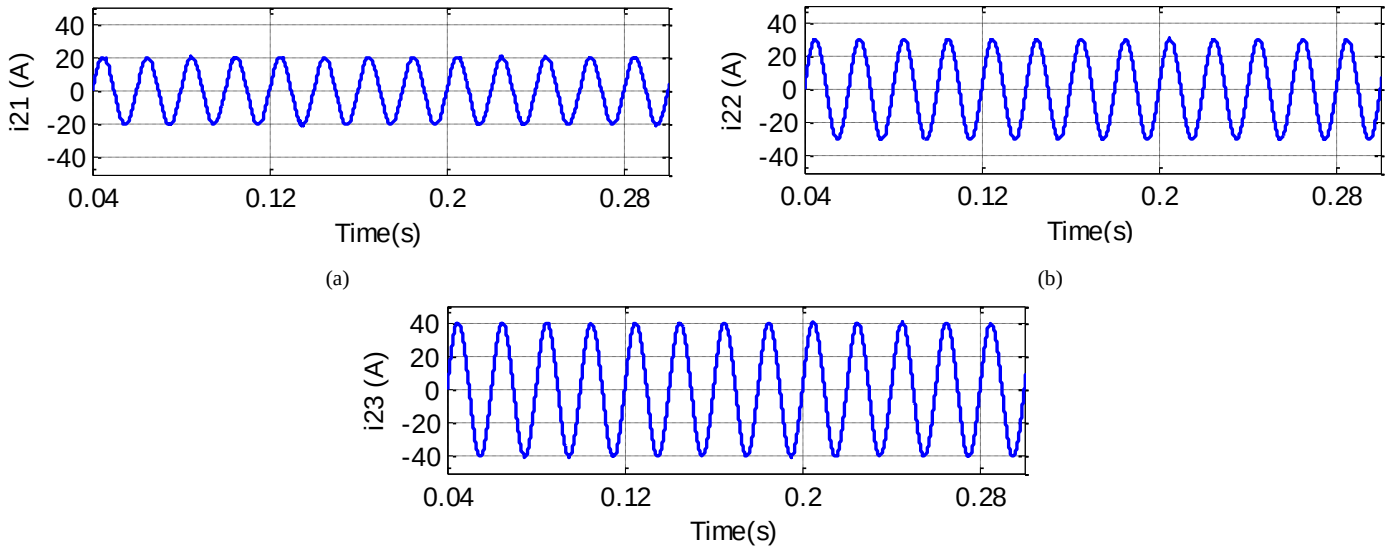

(a) (b)

(c)

Fig. 8. Simulated waveforms for single grid-connected inverter without considering the coupling effect of the inverters in design of controller parameters. (a) Inverter1 (b) Inverter2 (c) Inverter3.

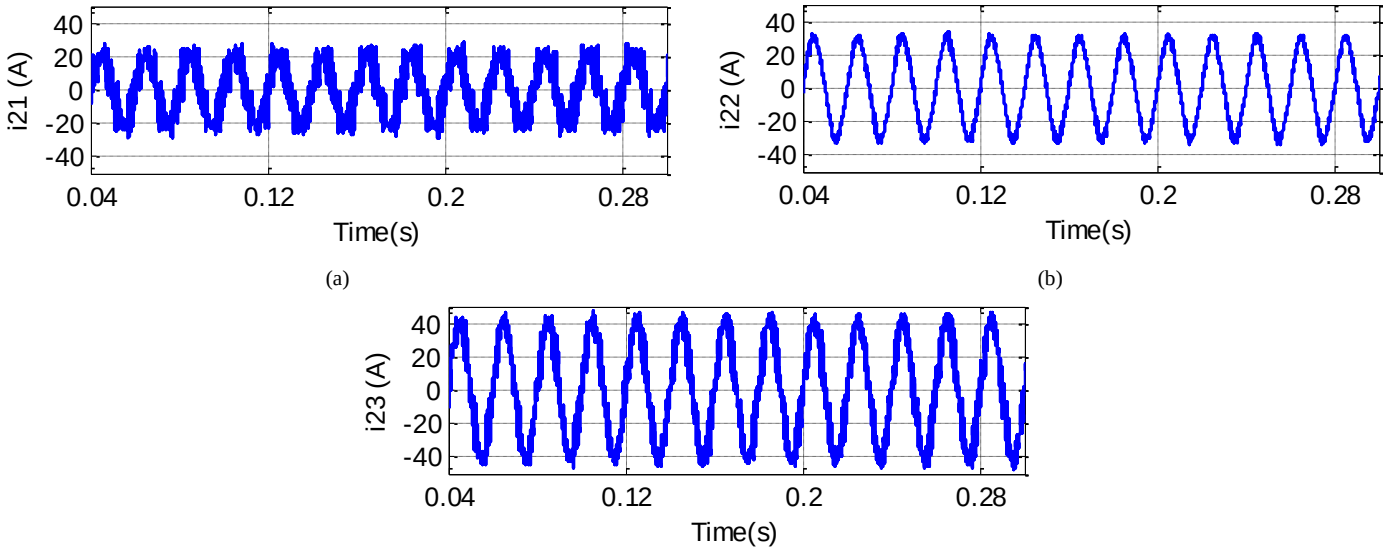

(a) (b)

(c)

Fig. 9. Simulated waveforms for multi-paralleled grid-connected inverters without considering the coupling effect of the inverters in design of controller parameters. (a) Inverter1 (b) Inverter2 (c) Inverter3.

In the next step, Set II control parameters listed in Table II is used for simulation. The controller parameters are designed with considering of coupling effect as shown in Fig. 7 for each inverter. In this paper, the inner loop cut-off frequencies of the inverter systems are designed 650 Hz, 700 Hz and 800 Hz, respectively. Also, the outer loop cut-off frequencies of the inverter systems are designed 500 Hz, 250 Hz and 500 Hz, respectively, with the PM of 80°.

The open-loop bode diagrams of the control system in Fig. 7 for each inverter are plotted in Figs. 10(a)-(c), respectively. It can be observed that with active damping, the resonance of the *LCL* filter is effectively damped and also, the loop gain at fundamental frequency (50 Hz) is higher than 150 dB for all three systems, which ensures the tracking error of the injected grid current is less than 1% thanks to PR controllers. According to Figs. 10(a)-(c), the three systems have cut-off frequency about 500 Hz, 250 Hz and 500 Hz, respectively with PM of about 80°.

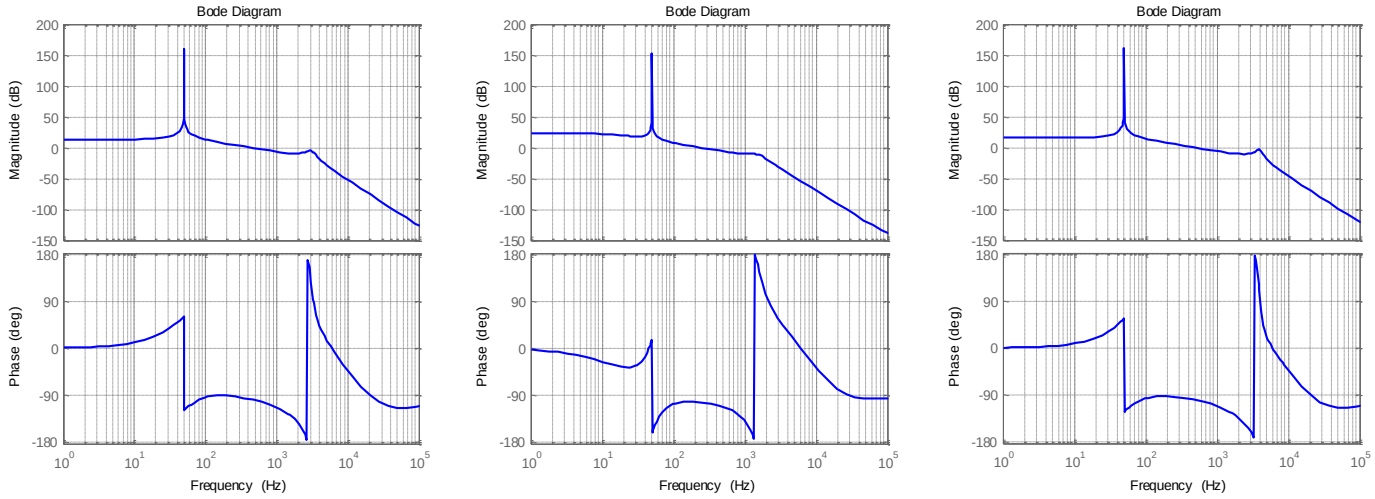

(a) (b) (c)

Fig. 10. Open loop bode diagram of the control systems (a) Inverter1. (b) Inverter2 (c) Inverter3.

The injected current of three inverters are shown in Figs. 11(a)-(c). It can be seen that, despite of differences in inverters and their control parameters, injected currents track the reference values. Also, THD of each inverter injected current and total injected current are 3.33%, 0.78%, 1.51% and 1.17%, respectively. Figure 11(d) shows the total grid-injected current which is exactly in phase with the PCC voltage and tracks the sum of reference currents thanks to PR controllers. The grid inductance (L_g) is selected a high value intentionally to simulate a weak grid. However, due to adequate control system design, this inductance reduces the harmonic distortion of the total grid-injected current as shown in Fig. 11(d).

To analyze the coupling effect of grid impedance and in order to validate control system performance, a step change occurs in the reference current of each inverter in different times. The reference current of inverter1 is reduced by 50% at t=0.105(s). The reference current of inverter2 is increased by 50% at t=0.205(s). The reference current of inverter3 is reduced by 50% at t=0.305(s). The simulation results using Set I control parameters in Table II are shown in Figs. 12(a)-(d). As shown in this figures, the grid-injected current of each inverter and also, the total grid-injected current are distorted and thier quality are not acceptable at all. Also, PCC voltage is distorted seriously, which affects connected loads at the PCC.

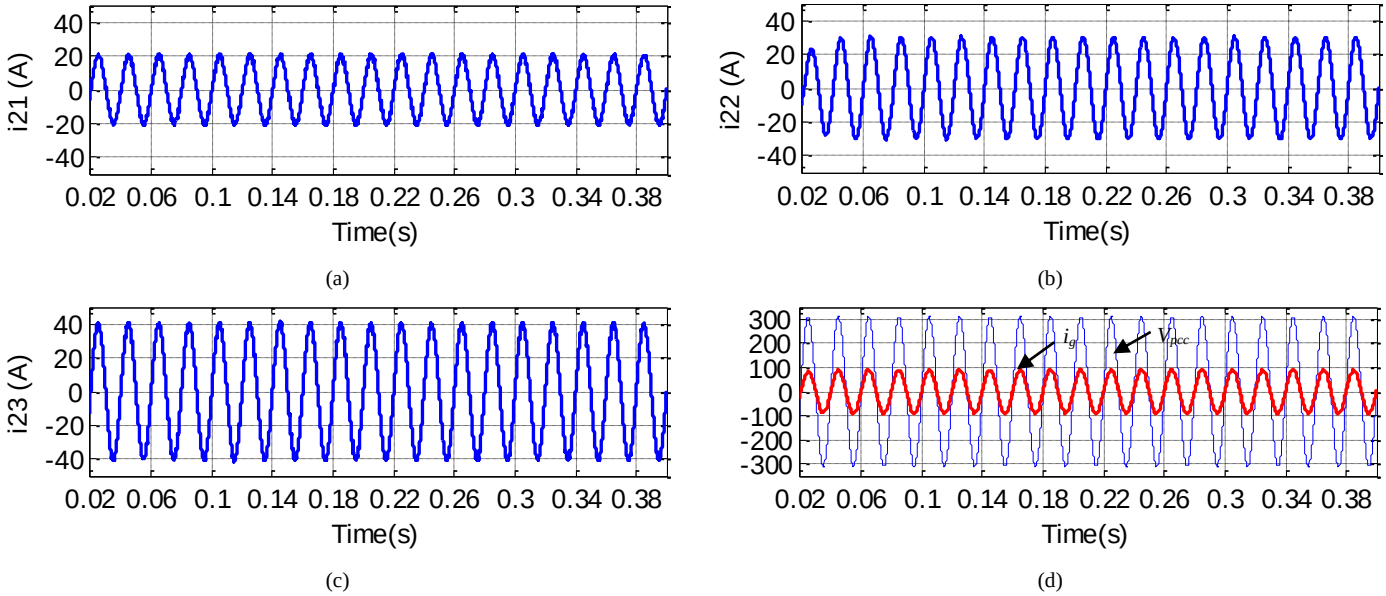

(a) (b) (c) (d)

Fig. 11. Simulated waveforms for multi-paralleled grid-connected inverters with considering the coupling effect of the inverters in design of controller parameters. (a) Inverter1. (b) Inverter2. (c) Inverter3. (d) Total injected current (i_g) and PCC voltage (V_{pcc}).

The simulation is repeated using Set II control parameters in Table II and its results are shown in Figs. 13(a)-(d). It can be seen that despite of step change in the reference current of each inverter, other inverters track their own reference currents with negligible disturbances in specified time. Also, total injected current tracks the sum of reference currents exactly without any instability which validates the proposed control system despite of inverters with different characteristics.

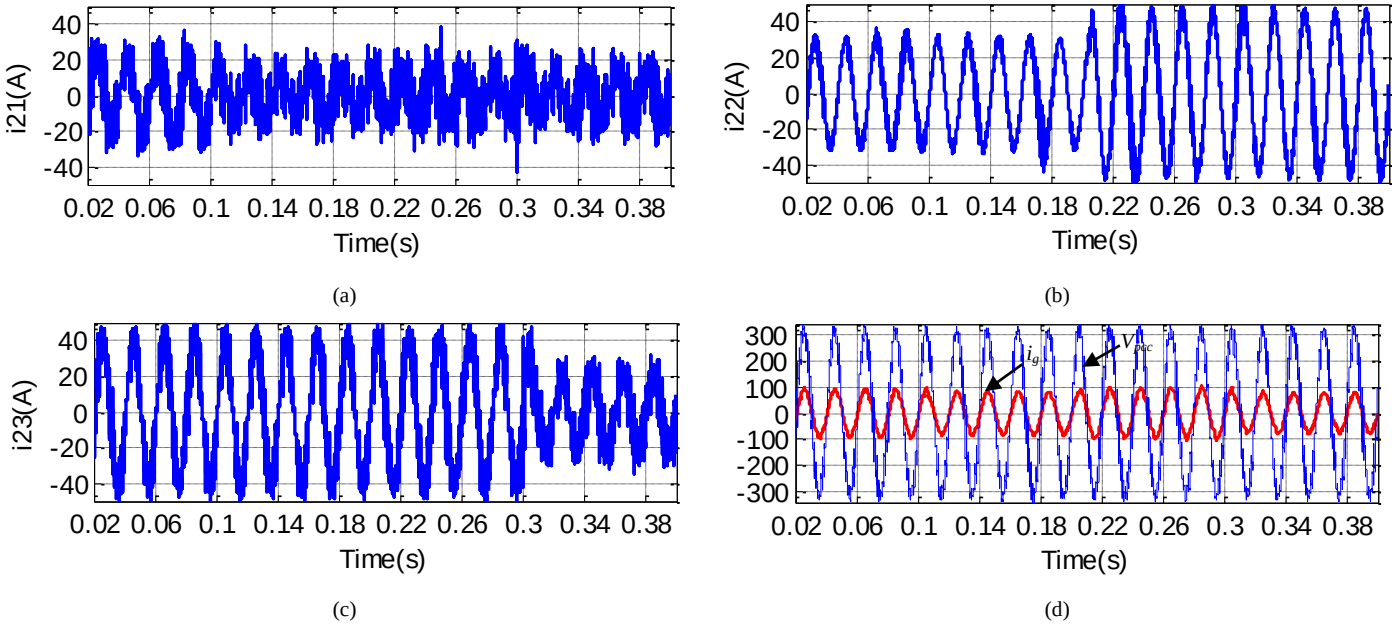

Fig. 12. Simulated waveforms with a step change in the reference current without considering the coupling effect of the inverters in design of controller parameters. (a) Inverter1. (b) Inverter2. (c) Inverter3. (d) Total injected current (i_g) and PCC voltage (V_{pcc}).

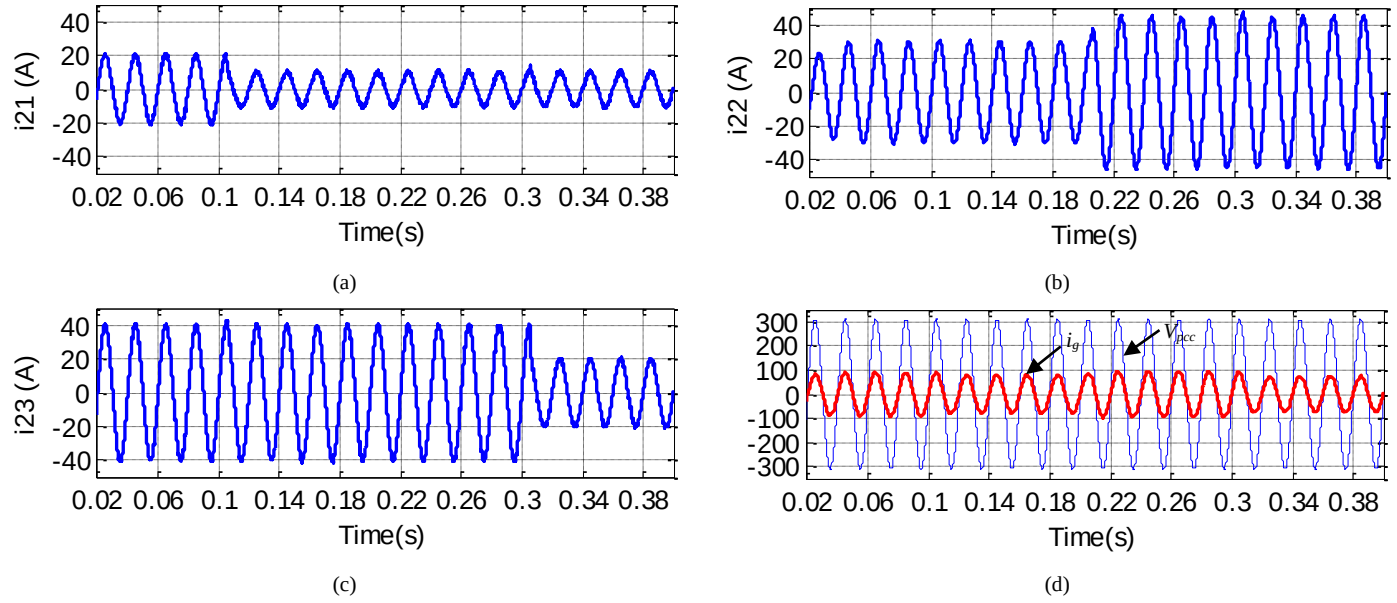

Fig. 13. Simulated waveforms with a step change in the reference current with considering the coupling effect of the inverters in design of controller parameters. (a) Inverter1. (b) Inverter2. (c) Inverter3. (d) Total injected current (i_g) and PCC voltage (V_{pcc}).

6. Conclusion

This paper analyses the modeling and design of a multivariable control system for multi-paralleled grid-connected inverters with *LCL* filter in a microgrid. The coupling effect due to grid impedance is described and dual-loop active damping control with capacitor current feedback is used to damp the *LCL* filter resonances. The inverters are modeled as a multivariable system considering the different characteristics for inverters such as *LCL* filters and rated powers. Three paralleled single-phase grid-

connected inverters are considered as a case study. Then, the control system design guidelines are suggested based on multivariable control theory. By using the PR controllers, the performance of the control system is improved. Simulation results of three-paralleled grid-connected inverters with *LCL* filter, in different conditions, confirm the validity of the modeling and effectiveness of the proposed control system.

Appendix

$$G_{11}=\frac{i_{11}}{v_{inv1}}=\frac{1}{Z_{11}+\left(Z_g\left\|\left[Z_{23}+\left(Z_{13}\left\|Z_{33}\right.\right)\right]\right\|\left[Z_{22}+\left(Z_{12}\left\|Z_{32}\right.\right)\right]+Z_{21}\right)\left\|Z_{31}\right.}$$

$$G_{12}=\frac{i_{11}}{v_{inv2}}=\frac{1}{\left(1+\frac{Z_{12}}{Z_{32}}+\frac{Z_{12}}{Z_{22}}\right)\left[-\left(1+\frac{Z_{22}}{Z_{21}}+\frac{Z_{22}}{Z_g\left\|\left[Z_{23}+\left(Z_{13}\left\|Z_{33}\right.\right)\right]\right.}\right)\left(Z_{11}+Z_{21}+\frac{Z_{11}Z_{21}}{Z_{31}}\right)+\frac{Z_{11}Z_{22}}{Z_{21}}\right]+\frac{Z_{12}}{Z_{22}}\left(Z_{11}+Z_{21}+\frac{Z_{11}Z_{21}}{Z_{31}}\right)}$$

$$G_{13}=\frac{i_{11}}{v_{inv\_3}}=\frac{1}{\left(1+\frac{Z_{13}}{Z_{33}}+\frac{Z_{13}}{Z_{23}}\right)\left[-\left(1+\frac{Z_{23}}{Z_{21}}+\frac{Z_{23}}{Z_g\left\|\left[Z_{22}+\left(Z_{12}\left\|Z_{32}\right.\right)\right]\right.}\right)\left(Z_{11}+Z_{21}+\frac{Z_{11}Z_{21}}{Z_{31}}\right)+\frac{Z_{11}Z_{23}}{Z_{21}}\right]+\frac{Z_{13}}{Z_{23}}\left(Z_{11}+Z_{21}+\frac{Z_{11}Z_{21}}{Z_{31}}\right)}$$

$$G_{21}=\frac{i_{12}}{v_{inv\_1}}=\frac{1}{\left(1+\frac{Z_{11}}{Z_{31}}+\frac{Z_{11}}{Z_{21}}\right)\left[-\left(1+\frac{Z_{21}}{Z_{22}}+\frac{Z_{21}}{Z_g\left\|\left[Z_{23}+\left(Z_{13}\left\|Z_{33}\right.\right)\right]\right.}\right)\left(Z_{12}+Z_{22}+\frac{Z_{12}Z_{22}}{Z_{32}}\right)+\frac{Z_{12}Z_{21}}{Z_{22}}\right]+\frac{Z_{11}}{Z_{21}}\left(Z_{12}+Z_{22}+\frac{Z_{11}Z_{22}}{Z_{32}}\right)}$$

$$G_{22}=\frac{i_{12}}{v_{inv\_2}}=\frac{1}{Z_{12}+\left(Z_g\left\|\left[Z_{23}+\left(Z_{13}\left\|Z_{33}\right.\right)\right]\right\|\left[Z_{21}+\left(Z_{11}\left\|Z_{31}\right.\right)\right]+Z_{22}\right)\left\|Z_{32}\right.}$$

$$G_{23}=\frac{i_{12}}{v_{inv\_3}}=\frac{1}{\left(1+\frac{Z_{13}}{Z_{33}}+\frac{Z_{13}}{Z_{23}}\right)\left[-\left(1+\frac{Z_{23}}{Z_{22}}+\frac{Z_{23}}{Z_g\left\|\left[Z_{21}+\left(Z_{11}\left\|Z_{31}\right.\right)\right]\right.}\right)\left(Z_{12}+Z_{22}+\frac{Z_{12}Z_{22}}{Z_{32}}\right)+\frac{Z_{12}Z_{23}}{Z_{22}}\right]+\frac{Z_{13}}{Z_{23}}\left(Z_{12}+Z_{22}+\frac{Z_{12}Z_{22}}{Z_{32}}\right)}$$

$$G_{31}=\frac{i_{13}}{v_{inv\_1}}=\frac{1}{\left(1+\frac{Z_{11}}{Z_{31}}+\frac{Z_{11}}{Z_{21}}\right)\left[-\left(1+\frac{Z_{21}}{Z_{23}}+\frac{Z_{21}}{Z_g\left\|\left[Z_{22}+\left(Z_{12}\left\|Z_{32}\right.\right)\right]\right.}\right)\left(Z_{13}+Z_{23}+\frac{Z_{13}Z_{23}}{Z_{33}}\right)+\frac{Z_{13}Z_{21}}{Z_{23}}\right]+\frac{Z_{11}}{Z_{21}}\left(Z_{13}+Z_{23}+\frac{Z_{13}Z_{23}}{Z_{33}}\right)}$$

$$G_{32}=\frac{i_{13}}{v_{inv\_2}}=\frac{1}{\left(1+\frac{Z_{12}}{Z_{32}}+\frac{Z_{12}}{Z_{22}}\right)\left[-\left(1+\frac{Z_{22}}{Z_{23}}+\frac{Z_{22}}{Z_g\left\|\left[Z_{21}+\left(Z_{11}\left\|Z_{31}\right.\right)\right]\right.}\right)\left(Z_{13}+Z_{23}+\frac{Z_{13}Z_{23}}{Z_{33}}\right)+\frac{Z_{13}Z_{22}}{Z_{23}}\right]+\frac{Z_{12}}{Z_{22}}\left(Z_{13}+Z_{23}+\frac{Z_{13}Z_{23}}{Z_{33}}\right)}$$

$$G_{33}=\frac{i_{13}}{v_{inv\_3}}=\frac{1}{Z_{13}+\left(Z_g\left\|\left[Z_{21}+\left(Z_{11}\left\|Z_{31}\right.\right)\right]\right\|\left[Z_{22}+\left(Z_{12}\left\|Z_{32}\right.\right)\right]+Z_{23}\right)\left\|Z_{33}\right.}$$

References

[1] D. Yang, X. Ruan, and H. Wu, "Impedance Shaping of the Grid-Connected Inverter with *LCL* Filter to Improve Its Adaptability to the Weak Grid Condition," *IEEE Trans. Power Electron.*, vol. 29, no. 11, pp. 5795–5805, Nov. 2014.

[2] G. Shen, X. Zhu, J. Zhang, and D. Xu, "A new feedback method for PR current control of LCL-filter-based grid-connected inverter," *IEEE Trans. Ind. Electron.*, vol. 57, no. 6, pp. 2033–2041, Jun. 2010.

[3] S. Mariéthoz and M.Morari, "Explicit model-predictive control of a PWM inverter with an *LCL* filter," *IEEE Trans. Ind. Electron.*, vol. 56, no. 2, pp. 389–399, Feb. 2009.

[4] W. Li, X. Ruan, D. Pan, and X. Wang, "Full-Feedforward Schemes of Grid Voltages for a Three-Phase *LCL*-Type Grid-Connected Inverter," *IEEE Trans. Ind. Electron.*, vol. 60, no. 6, pp. 2237–2250, June 2013.

[5] E. Twining and D. G. Holmes, "Grid current regulation of a three-phase voltage source inverter with an *LCL* input filter," *IEEE Trans. Power Electron.*, vol. 18, no. 3, pp. 888–895, May 2003.

[6] M. Liserre, F. Blaabjerg, and S. Hansen, "Design and control of an *LCL* filter-based three-phase active rectifier," *IEEE Trans. Ind. Appl.*, vol. 41, no. 5, pp. 1281–1291, Sep./Oct. 2005.

[7] J. Dannehl, F.W. Fuchs, S. Hansen, and P. B. Thøgersen, "Investigation of active damping approaches for PI-based current control of grid-connected pulse width modulation converters with *LCL* filters," *IEEE Trans. Ind. Appl.*, vol. 46, no. 4, pp. 1509–1517, Jul./Aug. 2010.

[8] M. Malinowski and S. Bernet, "A simple voltage sensorless active damping scheme for three-phase PWM converters with an *LCL* filter," *IEEE Trans. Ind. Electron.*, vol. 55, no. 4, pp. 1876–1880, Apr. 2008.

[9] IEEE Standard for Interconnecting Distributed Resources With Electric Power Systems, IEEE Std. 1547–2003, Jul. 28, 2003.

[10] J. L. Agorreta, M. Borrega, J. López, and L. Marroyo, "Modeling and Control of *N*-Paralleled Grid-Connected Inverters With *LCL* Filter Coupled Due to Grid Impedance in PV Plants," *IEEE Trans. Power Electron.*, vol. 26, no. 3, pp. 770–785, March 2011.

[11] J. He and Y. W. Li, "Generalized Closed-Loop Control Schemes with Embedded Virtual Impedances for Voltage Source Converters with *LC* or *LCL* Filters," *IEEE Trans. Power Electron.*, vol. 27, no. 4, pp. 1850–1861, April 2012.

[12] J. Xu, S. Xie, and T. Tang, "Active Damping-Based Control for Grid-Connected *LCL*-Filtered Inverter With Injected Grid Current Feedback Only," *IEEE Trans. Ind. Electron.*, vol. 61, no. 9, pp. 4746–4758, Sept. 2014.

[13] M. Hanif, V. Khadkikar, W. Xiao, and J. L. Kirtley, "Two Degrees of Freedom Active Damping Technique for LCL Filter-Based Grid Connected PV Systems," *IEEE Trans. Ind. Electron.*, vol. 61, no. 6, pp. 2795–2803, June 2014.

[14] A. Kahrobaeian and Y. A. R. I. Mohamed, "Robust Single-Loop Direct Current Control of *LCL*-Filtered Converter-Based DG Units in Grid-Connected and Autonomous Microgrid Modes," *IEEE Trans. Power Electron.*, vol. 29, no. 10, pp. 5605–5619, Oct. 2014.

[15] X. Li, X. Wu, Y. Geng, X. Yuan, C. Xia, and X. Zhang, "Wide Damping Region for *LCL*-Type Grid-Connected Inverter With an Improved Capacitor-Current-Feedback Method," *IEEE Trans. Power Electron.*, vol. 30, no. 9, pp. 5247–5259, Sept. 2015.

[16] S. Zhang, S. Jiang, X. Lu, B. Ge, and F. Z. Peng, "Resonance Issues and Damping Techniques for Grid-Connected Inverters With Long Transmission Cable," *IEEE Trans. Power Electron.*, vol. 29, no. 1, pp. 110–120, Jan. 2014.

[17] Y. Lei, W. Xu, C. Mu, Z. Zhao, H. Li, and Z. Li, "New Hybrid Damping Strategy for Grid-Connected Photovoltaic Inverter With *LCL* Filter," *IEEE Trans. Applied Supercond.*, vol. 24, no. 5, pp. 1–8, Oct. 2014.

[18] X. Chen, Y. Zhang, S. Wang, J. Chen, and C. Gong, "Impedance-Phased Dynamic Control Method for Grid-Connected Inverters in a Weak Grid," *IEEE Trans. Power Electron.*, vol. 32, no. 1, pp. 274–283, Jan. 2017.

[19] M. M. Rezaei and J. Soltani, "A robust control strategy for a grid-connected multi-bus microgrid under unbalanced load conditions," *Int J Electric Power Energy Syst.*, vol. 71, pp. 68–76, Oct. 2015.

[20] R. Majumder and G. Bag, "Parallel operation of converter interfaced multiple microgrids," *Int J Electric Power Energy Syst.*, vol. 55, pp. 486–496, Feb. 2014.

[21] A. Khaki-Sedigh and B. Moaveni, Control configuration selection for multivariable plants. Springer, 2009, pp. 13–55.

[22] S. Golestan, M. Monfared, J. M. Guerrero, and M. Joorabian, "A D-Q synchronous frame controller for single-phase inverters," in *Proc. Power Electronics, Drive Systems and Technologies Conference (PEDSTC), 2011 2nd*, Tehran, 2011, pp. 317–323.

[23] Bong-Hwan Kwon, Jin-Ha Choi and Tae-Won Kim, "Improved single-phase line-interactive UPS," *IEEE Trans. Ind. Electron.*, vol. 48, no. 4, pp. 804–811, Aug 2001.

[24] N. Zhang, H. Tang, and C. Yao, "A Systematic Method for Designing a PR Controller and Active Damping of the LCL Filter for Single-Phase Grid-Connected PV Inverters," Energies, vol. 7, no. 6, pp. 3934-3954, June 2014.